Narrow-band oscillations in probabilistic cellular automata

Marko Puljic* and Robert Kozma†
Department of Mathematical Sciences, University of Memphis, Memphis, Tennessee 38152-3240, USA
(Received 10 October 2007; revised manuscript received 23 May 2008; published 26 August 2008)

Dynamical properties of neural populations are studied using probabilistic cellular automata. Previous work demonstrated the emergence of critical behavior as the function of system noise and density of long-range axonal connections. Finite-size scaling theory identified critical properties, which were consistent with properties of a weak Ising universality class. The present work extends the studies to neural populations with excitatory and inhibitory interactions. It is shown that the populations can exhibit narrow-band oscillations when confined to a range of inhibition levels, with clear boundaries marking the parameter region of prominent oscillations. Phase diagrams have been constructed to characterize unimodal, bimodal, and quadromodal oscillatory states. The significance of these findings is discussed in the context of large-scale narrow-band oscillations in neural tissues, as observed in electroencephalographic and magnetoencephalographic measurements.

DOI: 10.1103/PhysRevE.78.026214 PACS number(s): 82.40.Bj, 84.35.+i, 05.50.+q

I. INTRODUCTION

In neural tissues, populations of neurons send electric currents to each other and produce activation potentials. While single unit activations have large variability and do not seem synchronous, the activations of neural assemblies often exhibit synchrony [1–4]. Ordinary and partial differential equations are widely used for modeling complex dynamics, including chaos and chaotic itinerancy [5,6]. The neural dynamics of spatially extended systems with small-world properties has been studied extensively [7–15]. The function-follow-form concept [16,17] is crucial for assessing the relation between the network structure and functioning of the neural tissue; for comprehensive models using differential equations, see [18–20]. Hierarchical models of the central nervous system based on ordinary differential equations with distributed parameters have been successfully applied to describe sensory processing and cognitive functions [1,21–23].

In this work we pursue an alternative approach, which uses probabilistic cellular automata to model cortical neural populations. Probabilistic cellular automata (PCA) are lattice models of spatially extended systems with probabilistic local dynamical rules of evolution [24]. PCA generalize deterministic cellular automata, such as Conway's game of life and cellular nonlinear networks (CNNs) [25], and bootstrap percolation where the update rule is deterministic but the initial configuration is random [26–31]. PCA often display very complex behaviors which are difficult to analyze rigorously [32]. Computational simulations provide an alternative tool of the analysis of the behavior of PCA in situations, which do not allow an analytical approach at present. In particular, critical behaviors in various PCA have been successfully analyzed using finite size scaling theory [33–35]. This is the route followed in the present work.

PCA often define a local neighborhood in their evolution rule, although this does not have to be the case in general [32,36]. Biological neurons have long-range connections via long axons which go far beyond their immediate dendritic arbors [37]. To describe such neural effects, we have developed PCA models incorporating mixed local and global (long-range) interactions. Binder's finite size scaling theory has shown that local-global PCA demonstrate behavior consistent with a weak Ising universality class [38–40]. The role of nonlocal interactions has been extensively studied in deterministic models, such as coupled map lattices (CMLs) [41,42]. CMLs with local-global coupling show critical behavior similar to PCA during transitions to synchronous chaos [9].

The present work extends PCA studies to more realistic systems with inhibitory effects. The cortical tissue contains two basic types of interactions: excitatory and inhibitory ones. Increased activities of excitatory populations influence positively (excite) their neighbors, while highly active inhibitory populations contribute negatively to (inhibit) the neurons they interact with. Inhibitory effects lead to the emergence of sustained narrow-band oscillations in the neural tissue, which are preconditions of the emergence of more complex, multicomponent brain rhythms [1,43–45]. Here we study families of PCAs with narrow-band oscillations, which serve as building blocks of large-scale random network models of brains [46].

This paper is organized as follows. First, basic concepts of probabilistic cellular automata are introduced, and critical behavior is characterized using Binder's finite-size scaling theory. Next, we extend the model to a two-layer PCA with excitatory and inhibitory populations. It is shown that PCA with inhibition can exhibit narrow-band oscillations, depending on the strength of inhibition. We analyze the conditions of the emergence of narrow-band oscillations, with bimodal probability distribution functions, as well as conditions of multimodal oscillations. Finally, we interpret these findings in the context of neural dynamics.

II. OVERVIEW OF CRITICALITY IN SINGLE-LAYER EXCITATORY PCA

A. Preliminaries on PCA with local neighborhoods

Here we summarize the terminology and previous results relevant to the present work [39]. Two-dimensional square

*neuropercolation@yahoo.com
†rkozma@memphis.edu; http://cnd.memphis.edu

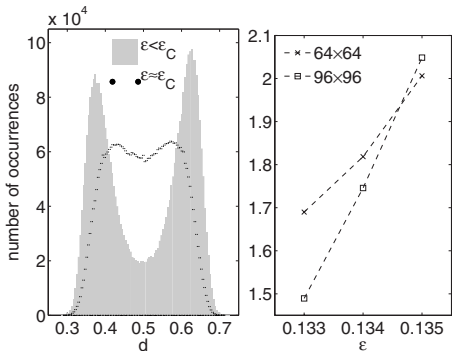

FIG. 1. Critical behavior for a single-layer PCA with local neighborhood. Left: activity distributions. Right: U^* values.

lattices are considered. The activation of the ith node at time t is denoted as $a_i(t)$, $t=1,2,3,\ldots,T$. Λ_i is the neighborhood of node i. Values of $a_i(t=0)$ are randomly initialized as 0 or 1, i.e., active or inactive. After $t=0$, an update rule is applied simultaneously over all sites at discrete time steps. We apply the probabilistic majority rule, according to which the ith site next value $a_i(t+1)$ is equal to the majority of its neighbors with probability $1-\varepsilon$, and to the value of the minority with probability ε. In the case of finite lattices, periodic boundary conditions are used, so the layer is folded into a torus.

PCA with various update rules and neighborhoods have been studied extensively using renormalization group techniques [34,35,47] and Binder's method [33]. Example of the size invariance of quantity U^* is illustrated in Fig. 1 in the case of a local PCA. Quantity U^* is related to the kurtosis and it is defined as follows:

$$U^* = \frac{\langle |d - \langle d \rangle|^4 \rangle}{\langle (d^* - \langle d^* \rangle)^2 \rangle^2}. \tag{1}$$

Here $d^*=|d-0.5|$ and $d=\Sigma_i^T a_i/T$. At the critical point ε_C, U^* is the same for all layer sizes of the same topology [35]. This is the point where the activation densities randomly hover around 0.5 and activation density distributions are unimodal. For $\varepsilon<\varepsilon_C$, the sites are either mostly active or mostly inactive and the activation distributions are bimodal, as illustrated in the gray shaded histogram on the left panel of Fig. 1.

B. Critical behavior in PCA with mixed topology

In a lattice with mixed local and nonlocal topology, some connections are rewired, so nodes may acquire nonlocal neighbors. Various rewiring schemes exist in the literature, including quenched random replacement, annealed randomness, and edge swap [48,49]. Different rewiring schemes result in different dynamics over the lattice. We use so-called regular rewiring schemes [50], when each node has the same number of connections and maintains this property after rewiring. In a simple regular two-dimensional square lattice, we consider the case when every node has five connections, i.e., four links to its direct neighbors and one to itself. In the present work we use edge swap rewiring as illustrated in Fig. 2. First, a link between the two randomly chosen local

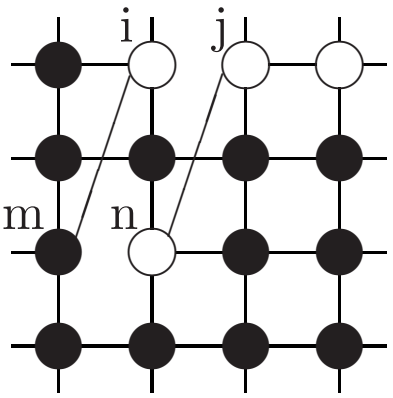

FIG. 2. Illustration of local and nonlocal links over a square lattice of size 4×4, $n_{NL}=25\%$.

neighbors, i and j, is removed. One of them, let us say i, is rewired to a randomly chosen site m. Next, one of m's local links is eliminated, i.e., the one going to n, to make sure that m has four neighbors. Now n has three neighbors, which is also true for the site j. To keep the number of neighbors per site constant, we connect n and j. This process is repeated until the desired number of nonlocal connections is reached. Based on biological motivation, a node can have at most one long-range connection. The relative importance of nonlocal links is defined as n_{NL} $=\{\text{No. nodes with nonlocal links}\}/\{\text{No. all nodes}\}\times100\%$.

RCA with mixed local and global neighborhoods show critical behavior and follow finite-size scaling laws [38,39]. Accordingly, magnetization d^* satisfies the relationship

$$d^* \propto (\varepsilon_C - \varepsilon)^\beta \quad \text{for } \varepsilon \to \varepsilon_C. \tag{2}$$

Similar scaling laws are valid for susceptibility χ and correlation length ξ:

$$\chi \sim |\varepsilon - \varepsilon_C|^{-\gamma}, \quad \xi \sim |\varepsilon - \varepsilon_C|^{-\nu} \quad \text{for } \varepsilon \to \varepsilon_C. \tag{3}$$

Critical exponents β, γ, and ν satisfy the hyperscaling identity $2\beta+\gamma=2\nu$ with good accuracy, indicating a behavior consistent with weak Ising universality class [39,40]. The critical exponents and the error of the identity $I_{\text{error}}=2\beta+\gamma-2\nu$ are reproduced in Table I; for details, see [39]. Note that results in Table I correspond to a bidirectional rewiring method used in [39], which is different from the edge swap technique adopted in this paper.

III. CRITICALITY IN THE PRESENCE OF INHIBITION

A. Structure of two-layer PCA

The two-layer PCA is illustrated in Fig. 3 with two bidirectional links from one layer to the other. Inhibition can be

TABLE I. Critical exponents in mixed models[a]

	ε_c	β	γ	ν	I_{error}
Local	0.1342	0.1308	1.8055	1.0429	0.02
25%(1)	0.1702	0.3071	1.1920	0.9504	0.09
100%(1)	0.2032	0.4217	0.9873	0.9246	0.02
100%(4)	0.2227	0.4434	0.9371	0.9026	0.02

[a]Reproduced from [39].

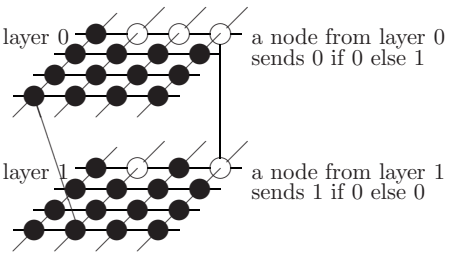

FIG. 3. PCA with two coupled local layers and n_X=12.5%.

modeled in various ways; here we introduce inhibition in the form of inverse influence, where one of the two layers is inversely influential (inhibitory). The excitatory layer operates as before and its nodes influence others with 1 when active and with 0 when inactive. A node from the inhibitory layer influences the node of the opposite layer in a reversed manner, i.e., with 1 when inactive, and with 0 when active. A constant size of neighborhood for all lattice points is maintained after rewiring in the two-layer configuration as well. Therefore a node loses a connection (its self-connection) when it is selected to receive a connection from the opposite layer. Parameter n_X defines the cross-layer coupling strength: n_X = {No. nodes with cross connection} / {No. all nodes} $\times 100\%$.

Typical behavior of a two-layer PCA in response to an excitatory impulse perturbation is illustrated in Fig. 4. A damped oscillation is observed as the result of excitatory-inhibitory interaction. Such a behavior is a basic building block of the dynamics of neural populations [1,23]. In response to the stimulus impulse, the excitatory cells reach a peak activation. The excitatory cells excite inhibitory cells, which reach a peak excitation a quarter of a cycle after the excitatory cells' peak activity (*a*). At this time, the excitatory cells are already inhibited to their basal, resting level. They reach maximum inhibition as the inhibitory cells return to their basal level (*b*). During this phase, the inhibitory cells receive diminishing excitation from the excitatory cells, so they undergo inhibition (*c*). When the excitatory cells are released from inhibition, they again respond to background activity, and start another cycle (*d*). A detailed quantitative analysis of critical properties of narrow-band oscillations in PCA is given in the next section.

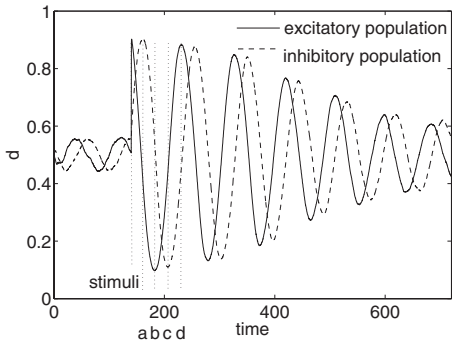

FIG. 4. Impulse response function of a PCA with excitatory and inhibitory layers. The phases of the damped oscillations are labeled as *a*, *b*, *c*, and *d*, and described in the text.

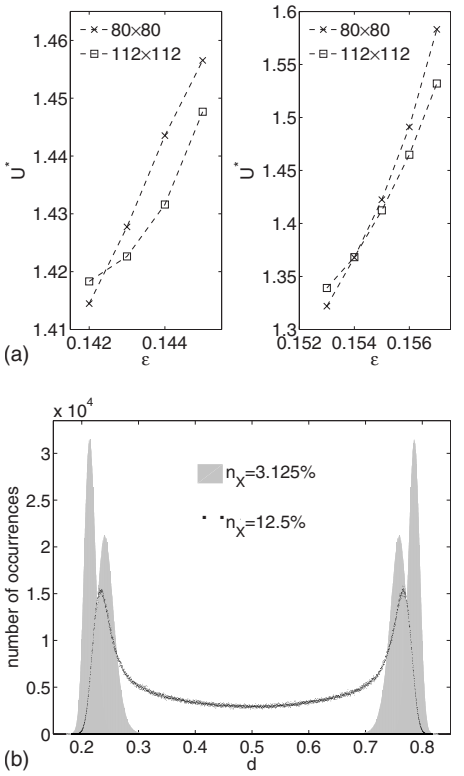

FIG. 5. Illustration of the onset of narrow-band oscillations at n_{NL}=25%. (a): U^* curves are displayed for system sizes 80×80 and 112×112, with n_X=3.125% (right) and 12.5% (left). (b): Activation distributions with n_X=3.125% (shade) and n_X=12.5% (dots).

B. Onset of narrow-band oscillations

The dynamical behavior of PCA changes drastically with the introduction of inhibitory connections, which can generate narrow-band oscillations, as well as more complex multimodal oscillations. When the noise level ε is varied while all other parameters are fixed, two critical points have been identified: ε_O and ε_C. ε_O marks the onset of prominent narrow-band oscillations, while ε_C describes the transition point where narrow-band oscillations disappear. These two critical points are described in this section and in the following section, respectively.

First the behavior at critical point ε_C is studied. Measurements are based on computer simulations of lattice sizes between 64×64 and 128×128. Experiments have been conducted with a range of noise levels, for various coupled lattice topologies in terms of nonlocal connections n_{NL} and cross-layer connections n_X. To achieve proper statistical accuracy, experiments were run at least for 1×10^6 steps or until $\langle|0.5-d|\rangle<0.001$.

Figure 5 illustrates the onset of prominent oscillations in systems with n_{NL}=25%. Activation distributions are displayed for ε=0.1425 on the lower panel of Fig. 5. It is seen that for n_X=12.5% (dotted line) the PCA has a bimodal distribution and produces prominent narrow-band oscillations. The value ε=0.1425 describes criticality for the given topology with n_X=12.5%. At the same time, ε=0.1425 is far below criticality at n_X=3.125% (shade), in which case the PCA

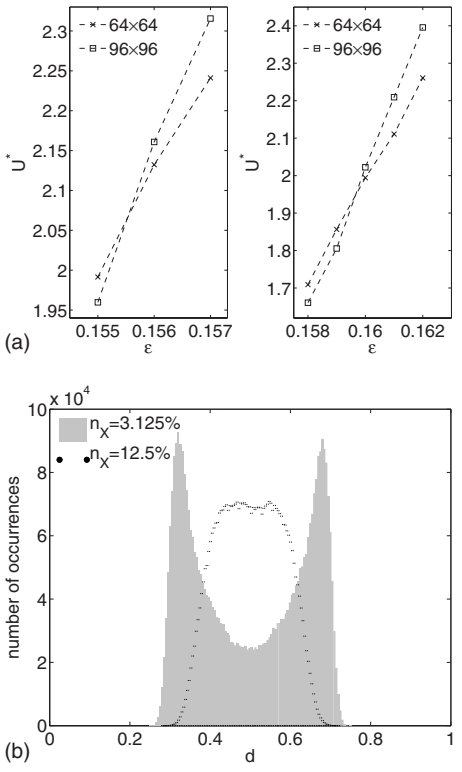

FIG. 6. Critical transitions from bimodal to unimodal states at $n_{NL}=25\%$. (a): U^* curves are displayed for system sizes 64×64 and 92×92, with $n_X=3.125\%$ (right) and 12.5% (left). (b): Activation distributions with $n_X=3.125\%$ (shade) and $n_X=12.5\%$ (dots).

has a more complex quadromodal distribution without narrow-band oscillations.

It is remarkable that U^* still provides suitable characterization of these systems, although the oscillations are significantly more complex than the single-layer homogeneous case, where kurtosis-based identification methods have been originally developed and applied [35]. The top two plots in Fig. 5 show U^* values for system size 80×80 (crosses) and 112×112 (squares). The curves intersect the first time when activation density distributions transform from quadromodal to bimodal distribution. This point is marked by ε_O. For given n_{NL}, ε_O decreases as n_X increases. This effect is discussed in detail below.

C. Critical transition from bimodal to unimodal state

Conditions resulting in diminishing prominent oscillations are studied here. ε_C denotes the critical ε value at which the distributions transit from bimodal to unimodal behavior; see Fig. 6. When ε increases and crosses the threshold ε_C, the bimodal activation density distribution transits to unimodal distribution. The distributions are obtained by simulating over 5×10^6 steps. This transition resembles critical phase transitions in single PCA layers, as illustrated in the top panels depicting the evolution of the kurtosis for systems of different sizes, 64×64 (cross) and 96×96 (square).

Coupled layers with the same connectivity parameters n_X and n_{NL} but with different system sizes display different U^* values if $\varepsilon\neq\varepsilon_O$; see Fig. 6, top left and right panels. For ε

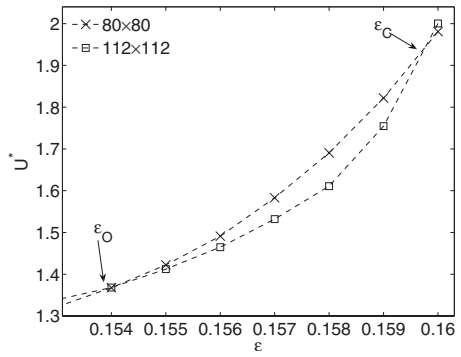

FIG. 7. Overview of the two types of transitions in the PCA with inhibition. The displayed U^* vs noise curves correspond to lattice sizes 80×80 and 112×112, respectively. The two curves intersect at two points indicated as ε_O and ε_C.

$<\varepsilon_O$, larger coupled layers have greater U^*. Immediately above ε_O, smaller systems have greater U^*. At ε_O, the U^* values are the same for any system size, which is an indication of critical behavior. We also observe (not shown here) that by increasing $\varepsilon>\varepsilon_O$, the frequency of the oscillations increases, while the distance between the peaks of the activation distribution decreases.

Figure 7 illustrates the quadromodal-to-bimodal and bimodal-to-unimodal transitions as ε varies over a wide range, for lattices with $n_{NL}=25\%$. This figure shows quadromodal-to-bimodal transition at $\varepsilon_0=0.1538$, and bimodal-to-unimodal transition at $\varepsilon_C=0.1596$. Prominent, narrow-band oscillations exist under the condition $\varepsilon_O<\varepsilon<\varepsilon_C$.

Figure 8 shows the dependence of critical noise values on the cross-layer connectivity n_X. The critical noise values decrease as n_X increases. The gap between ε_0 and ε_C is rather small for local lattice neighborhoods $n_{NL}=0$ (dotted lines), while it widens as n_{NL} increases, see $n_{NL}=25\%$ (dashed lines).

IV. DISCUSSIONS ON NARROW-BAND OSCILLATIONS IN PCA

PCA with excitatory and inhibitory connections exhibit more complex dynamic behavior than PCA with pure exci-

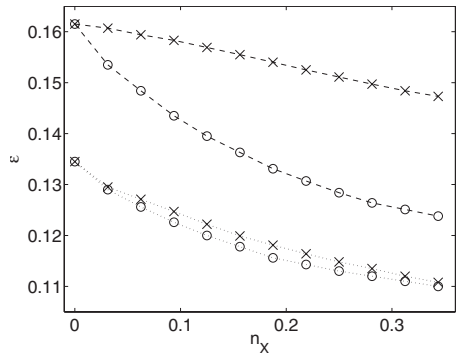

FIG. 8. Illustration of critical noise levels for lattices without rewiring (dotted lines at bottom) and with $n_{NL}=25\%$ (dash, top). Prominent bimodal oscillations exist between ε_O and ε_C curves, which are marked by circles and crosses, respectively.

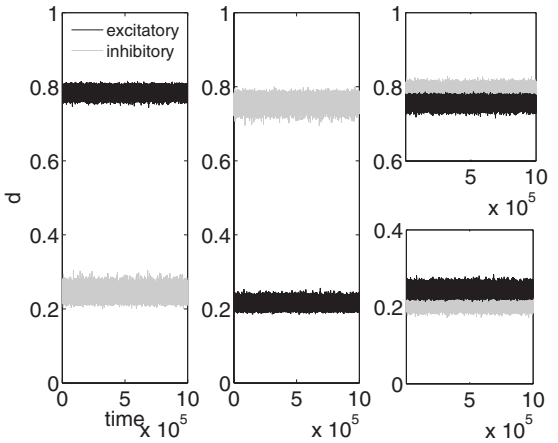

FIG. 9. Activation density of coupled layers with small $\varepsilon=0.1425$, $n_X=3.125\%$, and $n_{NL}=25\%$. This is a subcritical system with $\varepsilon<\varepsilon_O$ with quadromodal oscillations illustrated over four different time segments.

tatory connections. In particular, unimodal, bimodal, and quadromodal oscillations can be observed at various parameters when inhibition is present. Quadromodal oscillations are illustrated in Fig. 9, at various stages of the oscillatory cycle.

Starting with a mostly inactive inhibitory layer, this layer will mostly excite the opposite layer, and thus increases its average activation. Increasing activity in the excitatory layer excites the nodes linked in the inhibitory layer. The activation of the inhibitory layer increases, but it is less increased than the activation of the excitatory layer (Fig. 9, bottom right). The mostly active inhibitory layer inhibits the neighboring nodes in the excitatory layer and thus decreases its average activation. Decreased activity in the excitatory layer leads to the suppression of the excitation of the inhibitory layer. This time, the activation of the inhibitory layer is less suppressed then the activation of the opposite layer. The average activation of mostly active excitatory and mostly inactive inhibitory layers is higher than in the mostly active inhibitory and mostly inactive excitatory layers (Fig. 9 left and middle panels).

Figure 10 displays the phase diagram in the space of n_{NL} and ε. The diagram is shown for $n_X=3.125\%$, and $n_{NL}=25\%$, as an example. The regions corresponding to unimodal, bimodal, and quadromodal behaviors are labeled accordingly. The region with prominent bimodal oscillations is located between critical curves ε_C and ε_O. ε_C defines the separation between unimodal and bimodal regimes, while ε_O indicates bimodal-to-quadromodal transitions. Typical spatial distributions of activities are displayed for unimodal, bimodal, and quadromodal oscillations. The upper rows contain snapshots of excitatory layers, while lower rows show inhibitory layers.

Rigorous mathematical study of the observed phenomenon is very difficult and it is beyond the scope of this paper. Only very limited single-layer configurations allow thorough mathematical analysis at present, such as the mean field model, and the local model with weak noise [31,32]. Isotropic, mean field models in a single layer show that magnetization satisfies $d^*=f_m(d^*)$ [32], where

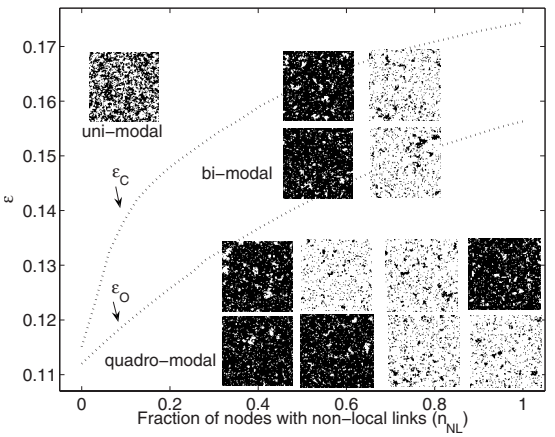

FIG. 10. Phase diagram in the space of n_{NL} and ε. The regions corresponding to unimodal, bimodal, and quadromodal behaviors are labeled accordingly. Typical spatial distributions of activities are displayed for excitatory (upper panel) and inhibitory (lower panel) layers, respectively. The separation between unimodal and bimodal regimes is defined by ε_C, while the bimodal-to-quadromodal transitions are demarcated by the curve given by ε_C. The diagram is evaluated for $n_x=3.125\%$, and $n_{NL}=25\%$.

$$f_m(x)=\sum_r \binom{|\Lambda|}{r} p_r x^r (1-x)^{|\Lambda|-r}. \tag{4}$$

For majority rule, $p_r=\varepsilon$ if $r<\Lambda/2$ and $p_r=1-\varepsilon$ if $r\geqslant\Lambda/2$. For a neighborhood of size $|\Lambda|=5$, the problem is analytically solvable and the critical exponent is $\beta=0.5$. The subcritical system is bistable and it has two symmetric fixed points between 0 and 1, due to the symmetry of the problem relative to 0.5. Adding nonlocal connections in a single-layer case changes the critical exponents and the critical points, but the system still exhibits transition between subcritical (paramagnetic) and supercritical (ferromagnetic) states, as observed in Ising systems [39].

In the presence of inhibition, the symmetry of the problem is broken and there can be multiple stable points and limit cycle solutions. With inhibition we have an extended critical region, not just a single critical point. The critical region is demarcated by ε_C and ε_O. Narrow-band oscillations take place under the condition $\varepsilon_C<\varepsilon<\varepsilon_O$. For supercritical regimes $\varepsilon>\varepsilon_O$, paramagnetic behavior is observed, while there are multimodal oscillations for subcritical parameters $\varepsilon_C>\varepsilon$. Mathematical analysis of these systems is the objective of ongoing efforts [51].

V. CONCLUSIONS

In this paper the presence of a two-step transition to criticality is demonstrated in PCA with inhibition. Our analysis is based on finite-scale scaling methodology applied to large-scale simulations. In coupled layers with appropriately selected topology and ε, the negative feedback from an inhibitory layer leads to the onset of narrow-band oscillations. These oscillations are very different from the ones observed in the case of pure excitation, when mutual excitation between the nodes maintains broadband oscillations, which are self-stabilized by a nonzero point attractor.

Noise values for the onset and termination of narrow-band oscillations depend on the PCA connectivity, defined by the density of nonlocal connections n_{NL} and the strength of the connection between excitatory and inhibitory layers n_X. The observed behavior has been analyzed here and illustrated using a phase diagram over the space of parameters ε and n_{NL}.

Future work aims at coupling several excitatory-inhibitory layers oscillating at different frequencies. Such a complex model can give rise to emergent spatiotemporal behaviors with multiple competing oscillations to simulate oscillations in large-scale cortical structures.

ACKNOWLEDGMENTS

Discussions with Walter J. Freeman (U.C. Berkeley), Paul Balister (University of Memphis), and Béla Bollobás (University of Cambridge, UK) have been very instrumental for the present work. Useful comments by the reviewers helped to improve the paper and are greatly appreciated.

[1] W. J. Freeman, Sci. Am. **264**, 78 (1991).
[2] W. J. Freeman, Int. J. Bifurcation Chaos Appl. Sci. Eng. **2**, 451 (1992).
[3] D. A. Steyn-Ross, M. L. Steyn-Ross, J. W. Sleigh, M. T. Wilson, I. P. Gillies, and J. J. Wright, J. Biol. Phys. **31**, 547 (2005).
[4] C. J. Stam, M. Breakspear van Cappellen, A. M. van Walsum, and B. W. van Dijk, Hum. Brain Mapp **19**, 63 (2003).
[5] K. Aihara, T. Takebe, and M. Toyada, Phys. Lett. A **144**, 333 (1990).
[6] K. Kaneko and I. Tsuda, *Complex Systems: Chaos and Beyond. A Constructive Approach with Applications in Life Sciences* (Springer, Berlin, NY, 2001).
[7] L. F. Lago-Fernandez, R. Huerta, F. Corbacho, and J. A. Siguenza, Phys. Rev. Lett. **84**, 2758 (2000).
[8] M. Perc, New J. Phys. **7**, 252 (2005).
[9] P. M. Gade and C. H. Hu, Phys. Rev. E **73**, 036212 (2006).
[10] O. Sporns, Proc. Natl. Acad. Sci. U.S.A. **103**, 19219 (2006).
[11] M. Perc, Chaos, Solitons Fractals **31**, 280 (2007).
[12] M. Perc, Phys. Rev. E **76**, 066203 (2007).
[13] Maruthi Pradeep Kanth Jampa, A. R. Sonawane, P. M. Gade, and S. Sinha, Phys. Rev. E **75**, 026215 (2007).
[14] X. Sun, Q. L. Matjaz Perc, and J. Kurths, Chaos **18**, 023102 (2007).
[15] H. Riecke, A. Roxin, S. Madruga, and S. A. Solla, Chaos **17**, 026110 (2007).
[16] R. Segev, M. Benveniste, Y. Shapira, and E. Ben-Jacob, Phys. Rev. Lett. **90**, 168101 (2003).
[17] V. Volman, Phys. Biol. **2**, 98 (2005).
[18] P. A. Robinson, C. J. Rennie, and D. L. Rowe, Phys. Rev. E **65**, 041924 (2002).
[19] V. Jirsa, Neuroinformatics **2**, 183 (2004).
[20] V. Jirsa and A. McIntosh, *Handbook of Brain Connectivity* (Springer, Berlin, 2007).
[21] R. Kozma and W. J. Freeman, Int. J. Bifurcation Chaos Appl. Sci. Eng. **11**, 2307 (2001).
[22] R. Kozma, Chaos **13**, 1078 (2003).
[23] W. J. Freeman and H. Erwin, Freeman K-set. Scholarpedia (www.scholarpedia.org) 3, (2), 3238 (2008).
[24] G. Grinstein, C. Jayaprakash, and Y. He, Phys. Rev. Lett. **55**, 2527 (1985).
[25] L. O. Chua, *CNN. A Paradigm for Complexity* (World Scientific, Singapore, 1998).
[26] M. Aizerman and J. L. Lebowitz, J. Phys. A **21**, 3801 (1988).
[27] A. M. S. Duarte, Physica A **157**, 1075 (1989).
[28] J. Adler, Physica A **171**, 453 (1991).
[29] R. Schonmann, Ann. Probab. **20**, 174 (1992).
[30] T. M. Liggett, Ann. Appl. Probab. **5**, 613 (1995).
[31] B. Bollobás and O. Riordan, *Percolation* (Cambridge University Press, Cambridge, England, 2006).
[32] P. Balister, B. Bollobás, and R. Kozma, Random Struct. Algorithms **29**, 399 (2006).
[33] K. Binder, Z. Phys. B: Condens. Matter **43**, 119 (1981).
[34] C. H. Bennett and G. Grinstein, Phys. Rev. Lett. **55**, 657 (1985).
[35] D. Makowiec, Phys. Rev. E **60**, 3787 (1999).
[36] L. G. Morelli, G. Abrahamson, and M. Kuperman, Eur. Phys. J. B **38**, 495 (2004).
[37] V. Braitenberg and A. Schutz, *Cortex: Statistics and Geometry* (Springer, Berlin, 1998).
[38] R. Kozma, M. Puljic, P. Balister, B. Bollobás, and W. J. Freeman, Lect. Notes Comput. Sci. **3305**, 435 (2004).
[39] R. Kozma, M. Puljic, B. Bollobás, P. Balister, and W. J. Freeman, Biol. Cybern. **92**, 367 (2005).
[40] M. Puljic and R. Kozma, Complexity **10**, 42 (2005).
[41] S. Sinha, D. Biswas, M. Azam, and S. V. Lawande, Phys. Rev. A **46**, 6242 (1992).
[42] R. Kozma, Phys. Lett. A **244**, 85 (1998).
[43] I. Aradi, G. Barna, and P. Erdi, Int. J. Intell. Syst. **10**, 89 (1995).
[44] M. Arbib, P. Erdi, and J. Szentagothai, *Neural Organization* (MIT Press, Cambridge, MA, 1997).
[45] G. Buzsaki, *Rhythms of the Brain* (Oxford University Press, New York, 2006).
[46] R. Kozma, Neuropercolation. Scholarpedia (www.scholarpedia.org) 2(8), 1360 (2007).
[47] R. Cerf and E. N. Cirillo, Ann. Probab. **27**, 1837 (1999).
[48] G. Szabo, A. Szolnoki, and R. Izsak, J. Phys. A **37**, 2599 (2004).
[49] F. C. Santos, J. F. Rodrigues, and J. M. Pacheco, Phys. Rev. E **72**, 056128 (2005).
[50] X. Wang and G. Chen, IEEE Trans. Circuits Syst. **31**, 6 (2003).
[51] *Handbook of Large-Scale Random Networks*, Series: Bolyai Society Mathematical Studies, edited by B. Bollobás, R. Kozma, and D. Miklos, volume no. 18, (2008). (to be published).